AMERICAN SOCIETY FOR MICROBIOLOGY | Applied and Environmental Microbiology®

ENVIRONMENTAL MICROBIOLOGY

Coculturing Bacteria Leads to Reduced Phenotypic Heterogeneities

Jasmine Heyse,[a] Benjamin Buysschaert,[a] Ruben Props,[a] Peter Rubbens,[b] Andre G. Skirtach,[c] Willem Waegeman,[b] Nico Boon[a]

[a]Center for Microbial Ecology and Technology, Department of Biochemical and Microbial Technology, Ghent University, Ghent, Belgium
[b]KERMIT, Department of Data Analysis and Mathematical Modeling, Ghent University, Ghent, Belgium
[c]Nano-Bio-Technology Group, Department of Biotechnology, Ghent University, Ghent, Belgium

ABSTRACT Isogenic bacterial populations are known to exhibit phenotypic heterogeneity at the single-cell level. Because of difficulties in assessing the phenotypic heterogeneity of a single taxon in a mixed community, the importance of this deeper level of organization remains relatively unknown for natural communities. In this study, we have used membrane-based microcosms that allow the probing of the phenotypic heterogeneity of a single taxon while interacting with a synthetic or natural community. Individual taxa were studied under axenic conditions, as members of a coculture with physical separation, and as a mixed culture. Phenotypic heterogeneity was assessed through both flow cytometry and Raman spectroscopy. Using this setup, we investigated the effect of microbial interactions on the individual phenotypic heterogeneities of two interacting drinking water isolates. Through flow cytometry we have demonstrated that interactions between these bacteria lead to a reduction of their individual phenotypic diversities and that this adjustment is conditional on the bacterial taxon. Single-cell Raman spectroscopy confirmed a taxon-dependent phenotypic shift due to the interaction. In conclusion, our data suggest that bacterial interactions may be a general driver of phenotypic heterogeneity in mixed microbial populations.

IMPORTANCE Laboratory studies have shown the impact of phenotypic heterogeneity on the survival and functionality of isogenic populations. Because phenotypic heterogeneity plays an important role in pathogenicity and virulence, antibiotic resistance, biotechnological applications, and ecosystem properties, it is crucial to understand its influencing factors. An unanswered question is whether bacteria in mixed communities influence the phenotypic heterogeneity of their community partners. We found that coculturing bacteria leads to a reduction in their individual phenotypic heterogeneities, which led us to the hypothesis that the individual phenotypic diversity of a taxon is dependent on the community composition.

KEYWORDS Raman spectroscopy, axenic culture, coculture, flow cytometry, microbial interactions, phenotypic heterogeneity, single cell, synthetic ecosystems

Genetically identical bacteria are known to exhibit single-cell heterogeneity under controlled laboratory conditions (1–3). These heterogeneous traits include morphological traits, such as cell size, as well as biochemical properties, such as protein and mRNA content. The individualization of identical sister cells in clonal populations occurs rapidly after cell division (4). Cells can be partitioned into clusters of cells with similar traits, called phenotypes. The variation in phenotypes within sympatric isogenic populations is referred to as the phenotypic heterogeneity (5).

Noise in gene expression is known to be one of the main drivers of phenotypic heterogeneity (6–8). At first glance, a heterogeneous gene expression appears to be

Citation Heyse J, Buysschaert B, Props R, Rubbens P, Skirtach AG, Waegeman W, Boon N. 2019. Coculturing bacteria leads to reduced phenotypic heterogeneities. Appl Environ Microbiol 85:e02814-18. https://doi.org/10.1128/AEM.02814-18.

Editor Robert M. Kelly, North Carolina State University

Address correspondence to Nico Boon, Nico.Boon@UGent.be.

Received 22 November 2018
Accepted 11 February 2019
Accepted manuscript posted online 22 February 2019
Published 4 April 2019

disadvantageous, as it may reduce the mean fitness of the population under the prevailing environmental conditions (9). However, several studies have indicated that biological noise is an evolved and regulated trait (10, 11), which offers benefits for the survival (12, 13) and functionality (14–16) of a clonal population. The aforementioned studies have revealed that isogenic bacterial populations are not homogeneous populations. Instead, they behave as communities consisting of phenotypic subgroups, which may differ in quantitative (i.e., continuous variation in phenotypic traits) and qualitative (i.e., distinct phenotypic states) aspects.

In nature, bacteria are not encountered as isolated populations, but they are a part of a larger association where many microorganisms coexist. To date, little research has been devoted to the occurrence and functional consequences of phenotypic heterogeneity in natural, mixed communities (17, 18), and our knowledge regarding factors that influence phenotypic heterogeneity is limited. One of the reasons for this is that it is difficult to assess the heterogeneity of a single taxon within a mixed community. Recently, several experimental approaches that assess the metabolic diversity of a single taxon in natural communities have been developed (19, 20). However, these approaches rely on fluorescence in situ hybridization probes that bind to 16S rRNA gene sequences for identification of the taxon of interest. Hence, these approaches do not allow exclusion of the possibility that some of the observed phenotypic differences are caused by minor genetic differences between bacteria with very similar 16S rRNA genes.

Two laser-based methods that are suitable for assessing phenotypes are flow cytometry and Raman spectroscopy (21–23). Two types of light can be detected by the flow cytometer: scattered light and fluorescence. The scattered light provides information about the basic characteristics of the cells (e.g., size, shape, and surface properties), while the fluorescence data provide additional information about the cell properties for which it has been stained (e.g., nucleic acid content, metabolic activity, etc.) (24). Flow cytometry thus gives information regarding the morphological, as well as specific physiological, properties of single cells. The Raman spectrum of a single cell consists of a combination of the individual spectra of all the compounds that make up this cell (e.g., proteins, nucleic acids, fatty acids, etc.). This results in a complex spectrum, which can be interpreted as a chemical fingerprint of the cell (25, 26). Hence, single-cell Raman spectra offer an in-depth view on the biochemical composition of each phenotype.

A tool that can help to answer questions that are difficult to study directly in natural communities is a synthetic ecosystem. A synthetic ecosystem consists of a selected set of species under specific conditions. Such ecosystems are controllable and have a reduced complexity in comparison to natural communities (27). Hence, they provide a way to test ecological theories in order to better understand the rules of nature (28). A specific setup for these synthetic ecosystems is cocultures. The principle of such a system is that two or more bacterial populations are cultivated together with some degree of contact between them, which allows study of their interactions (29).

An unanswered question, and the focus of this study, is whether bacteria in mixed communities influence the phenotypic heterogeneity of their community partners. Here, we used a synthetic community setup where two isolates were used as model organisms. Four synthetic communities were created. The isolates were grown in axenic cultures as a reference for noninteracting genotypes. To be able to study the individual community members separately after they have been interacting via their joint medium, a coculture with physical separation by a membrane was created. Lastly, a mixed culture without physical separation, representing "full interaction," was created. Phenotypes were assessed through flow cytometry and single-cell Raman spectroscopy. Furthermore, we applied and evaluated a novel machine learning approach to quantify synthetic community composition through flow cytometric fingerprinting.

RESULTS

We aimed to evaluate whether the phenotypes and phenotypic heterogeneity of a single taxon in a dual-species coculture are mediated by interactions with a partner taxon. Two drinking water isolates, an *Enterobacter* sp. and a *Pseudomonas* sp., were

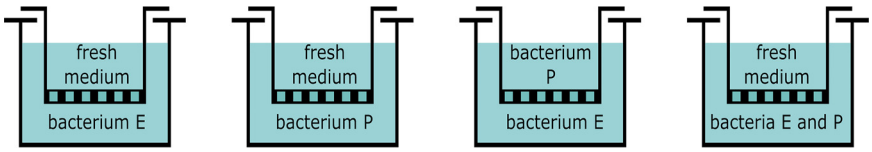

FIG 1 Illustration of the experimental setup. Bacteria in apical and basal phase can interact via metabolites in their shared medium while they are physically separated by the membrane of the cell culture inserts. Four synthetic communities were created: two axenic cultures, a coculture, and a mixed culture. There were biological replicates ($n = 3$) for each synthetic community.

used as model organisms. The experimental design consisted of four synthetic communities: two axenic cultures, a coculture with physical separation between the taxa (partial interaction), and a mixed culture (full interaction) (Fig. 1). Each synthetic community was prepared in triplicate, and the communities were monitored for 72 h. Every 24 h, the population phenotypic diversity was assessed by flow cytometry. At 72 h, populations were analyzed using single-cell Raman spectroscopy. Cell viability was verified through SYBR Green I (SG) and propidium iodide staining (see Fig. S1 in the supplemental material). Cell populations remained viable throughout the course of the experiment and differences in viability between the coculture and the axenic culture were insignificant for both taxa (Wilcoxon rank sum test, $P > 0.05$; Fig. S1). In the results presented below, the physically separated culture is referred to as the "coculture," while "mixed culture" indicates the culture without physical separation.

Flow cytometric diversity assessment. To evaluate whether microbial interactions can lead to changes in the phenotypic heterogeneity of interacting organisms, cytometric diversity estimates were used as measures of phenotypic heterogeneity. For this, an equal-spaced binning grid was used to arbitrarily split up the cytometric parameter space in operational phenotypic units. The signals of both scatter and fluorescence detectors were used, implying that the diversity is a measure of population heterogeneity in terms of both morphological traits and nucleic acid content. Note that the calculated diversity metrics are independent of the taxon abundances (Fig. S2), as all populations were subsampled to equal cell counts prior to diversity estimation (see Materials and Methods).

The phenotypic community structure was first investigated through an alpha diversity (i.e., within-sample diversity) assessment. For both taxa, the diversity of the individual taxon was larger when present in the axenic culture compared to when the same taxon was present as a member of the coculture. Not only the phenotypic diversity (D_1 and D_2), which includes both richness and evenness, decreased (Fig. S3), but the phenotypic richness (D_0) of the coculture members decreased compared to the axenic cultures (Fig. 2A). This indicates not only that the interaction led to a reorganization of the phenotypic community structure (i.e., a change in the relative abundances of the cytometric bins) but also that the number of nonempty bins on the cytometric fingerprint was reduced due to the interaction, implying not only a redistribution of trait abundance but also a reduction in trait heterogeneity. At 72 h, the alpha diversities (D_0) were significantly lower in the cocultures compared to the axenic cultures, for both *Enterobacter* (one-sided Wilcoxon rank sum test, $P = 0.05$) and *Pseudomonas* ($P = 0.05$). The phenotypic diversity metrics were not additive when compared between the two coculture members and the mixed culture, suggesting that fractions of these two populations share certain phenotypic properties.

Using a contrast analysis, differences between the phenotypic fingerprints of populations can easily be visualized in bivariate parameter spaces. To evaluate whether the observed lower diversities were linked with specific shifts in the cytometric fingerprint, differences in scatter and fluorescence patterns of the axenic cultures and the cocultures were assessed. The differences in scatter patterns were limited for both taxa (Fig. S4). In contrast, a clear difference in fluorescence intensity was observed (Fig. 2B and C; Fig. S5). For *Enterobacter* there was a shift toward high-fluorescence cells in the coculture compared to the axenic culture. This difference became larger over time. For

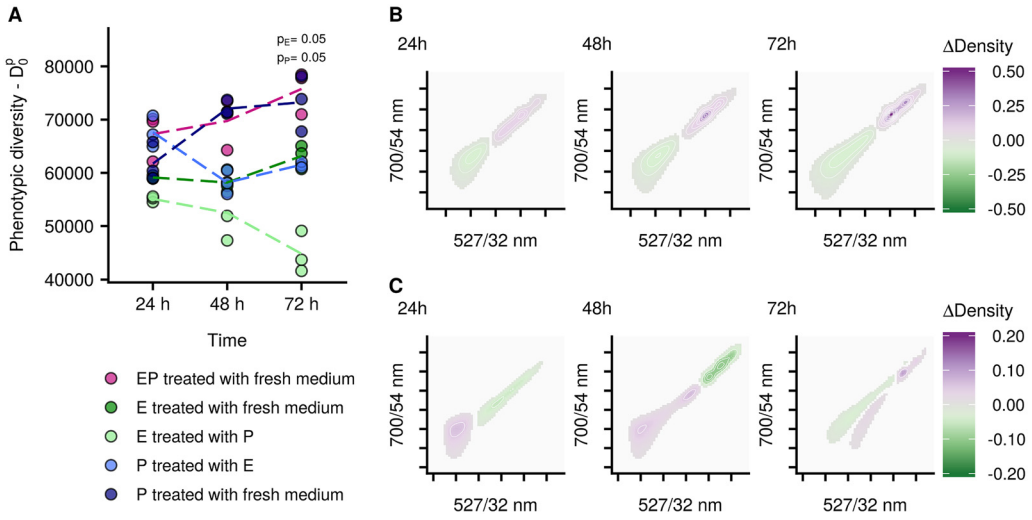

FIG 2 (A) Phenotypic alpha diversity D_0 for both individual bacterial taxa in communities of axenic cultures, cocultures, and mixed cultures. The taxa are denoted as taxon E (*Enterobacter* sp.) and taxon P (*Pseudomonas* sp.), respectively. The populations are indicated with names in the form of "X treated with Y," where X is the taxon in the sample (E, P, or EP) and Y is what was present on the other side of the membrane (E, P, or fresh medium). There were biological replicates ($n = 3$) for each community. The dashed lines indicate the average trend of the replicates. *P* values indicate the significance of the differences between the axenic culture and coculture populations at 72 h for *Enterobacter* (P_E) and *Pseudomonas* (P_P) (one-sided Wilcoxon rank sum test). (B and C) Contrast analysis of the phenotypic fingerprints was performed to compare the phenotypic community structure of axenic cultures and coculture members with respect to fluorescence intensity. Each plot is a comparison between the axenic culture and coculture of the same taxon at the same time point, averaged over the three biological replicates. The color gradient indicates whether density in the coculture increased (purple) or decreased (dark green) relative to their respective axenic culture at the specified time point. (B) The upper row presents contrast results for *Enterobacter*. (C) The lower row presents contrast results for *Pseudomonas*. If the difference between the two communities is <0.01, no contrast value is shown on the graphs, which causes the appearance of different clusters. Note that different scales were used for the different taxa.

Pseudomonas there was a more limited difference, with a small enrichment of lower-fluorescence cells. Thus, there was not only a reduction in population diversity, but there was also a shift of the population fingerprint. Moreover, this shift was taxon dependent.

To further compare the cytometric fingerprints of the different populations, a principal coordinate analysis (PCoA) ordination was generated based on the Bray-Curtis dissimilarities between the fingerprints (Fig. 3). In this ordination, the fingerprints of the taxa, both under axenic and under coculture growth, are separated, with the mixed culture in between. The populations show a significant shift in their phenotypic structure through time ($P = 0.001$, $r^2 = 0.154$). In addition, there is a significant difference in the fingerprint of *Enterobacter* when present as an axenic culture compared to being present in the coculture ($P = 0.001$, $r^2 = 0.455$). For *Pseudomonas*, the differences between the axenic cultures and coculture members were not significant ($P = 0.092$, $r^2 = 0.170$). The mixed culture shifted from a community that is more resembling *Enterobacter* at the first measurement, toward a community that is more similar to *Pseudomonas* at the second and third measurements.

To better understand the interaction that was occurring between *Enterobacter* and *Pseudomonas*, we applied a novel machine learning approach to infer the relative abundances of both taxa in the mixed community (30). Previous results confirmed our initial hypothesis that the phenotypic diversity of a taxon can be influenced by the presence of other taxa. In order to take this into account, a random forest classifier was trained, for each time point separately, on the fingerprints of the coculture members at the corresponding time point, as these are expected to be the most biologically accurate (see the supplemental results and discussion). The predictions indicate a higher abundance of *Enterobacter* in the community at 24 h, followed by a gradual enrichment of *Pseudomonas* at the second and third time points (Fig. 4). Classifier accuracy was always >94% (Table S1). The results of this study show that the pheno-

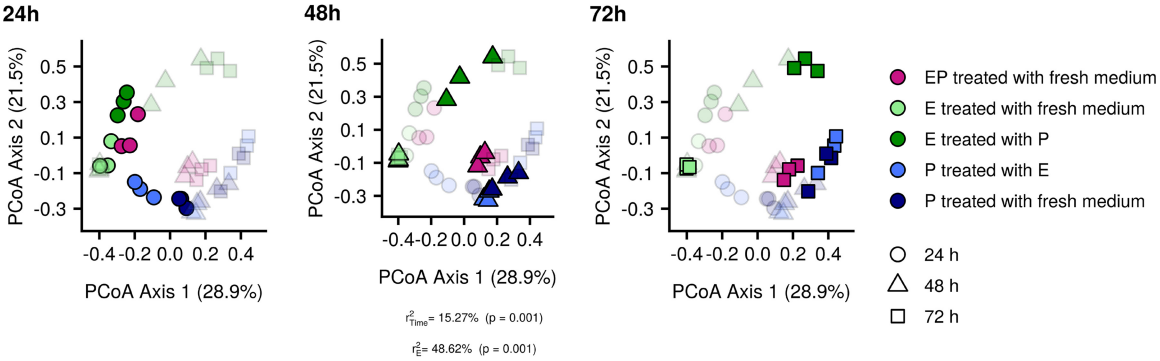

FIG 3 PCoA ordination of the Bray-Curtis dissimilarities between the phenotypic fingerprints for both individual bacterial taxa in communities of axenic cultures, cocultures, and mixed cultures. The ordination is shown in three graphs, split according to time, since this allows for easier interpretation of how the different communities are relating to each other at each time point. The taxa are denoted as taxon E (*Enterobacter* sp.) and taxon P (*Pseudomonas* sp.), respectively. The populations are indicated with names in the form of "X treated with Y," where X is the taxon in the sample (E, P, or EP) and Y is what was present on the other side of the membrane (E, P, or fresh medium). There were biological replicates ($n = 3$) for each community. The variance explained by the overall temporal effect (r^2_{Time}), as well as the effect of coculturing compared to axenic culture (r^2_E), is provided (PERMANOVA). The effect of coculturing was not significant for *Pseudomonas* and is therefore not indicated.

typic community structure of a taxon is a dynamic property, in time as well as in relation to external influencing factors such as presence of other taxa. Before further applying the *in silico* methodology to infer community composition of synthetic ecosystems, it is recommended to have an external validation of the predicted relative abundances (see the supplemental results and discussion).

In summary, both *Enterobacter* and *Pseudomonas* showed lower phenotypic diversities in the coculture compared to their axenic culture counterparts. However, while the overall phenotypic community structure did not change substantially for *Pseudomonas* (i.e., small differences in beta diversity and limited shift toward lower-fluorescence-intensity cells), there was a clear shift in the phenotypes of the *Enterobacter* population (i.e., large differences in beta diversity and a clear shift toward higher-fluorescence-intensity cells).

Raman phenotyping. The cytometric phenotype only takes into account the morphological characteristics and nucleic acid content of the cells. However, phenotypes can differ in more cell constituents than nucleic acids alone. The Raman spectrum of a single cell offers a more in-depth view on the biochemical phenotype compared to flow cytometry. Raman spectroscopy was used to measure single-cell spectra for each of the populations of *Enterobacter* and *Pseudomonas* in the axenic cultures and the coculture at 72 h.

The spectra hold 333 wavenumbers over the selected biologically relevant range. To gain insight in the separability of cells from the different populations, spectra were visualized through PCA after preprocessing of the data (see Materials and Methods) (Fig. 5A). The spectra of the *Enterobacter* populations were clearly separated. A large overlap between the spectra of *Pseudomonas* that was grown in axenic culture and *Pseudomonas* that was grown in the coculture was observed. However, when performing PCA for each taxon separately, cells from the coculture and the axenic culture were separated well (Fig. 5B and C). For *Enterobacter*, the axenic and coculture groups differed significantly ($P = 0.001$, $r^2 = 0.343$). For *Pseudomonas*, no permutational multivariate analysis of variance (PERMANOVA) could be performed since the group dispersions were significantly different. This confirms the previous results, indicating that for both taxa a phenotypic shift occurred but that this shift was larger for *Enterobacter* than for *Pseudomonas*.

Since the Raman spectrum of a single cell is a combination of the spectra of all compounds that make up this cell (e.g., proteins, nucleic acids, fatty acids, etc.), the signal intensity at every wavenumber is the result of all compounds that produce a signal at this wavenumber. The Raman spectra of all DNA and RNA bases are available

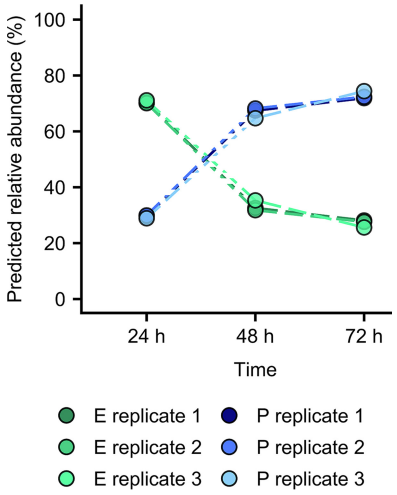

FIG 4 Predicted relative abundances in the mixed cultures. The random forest classifiers that were used to infer community composition were constructed using the fingerprints of the coculture members at the corresponding time point as input data. Green lines indicate the predicted relative abundances of *Enterobacter*; blue lines indicate the predicted relative abundances of *Pseudomonas*. The different shades correspond to biological replicates ($n = 3$).

from literature (31), as well as information regarding peak regions that are assumed to be related to nucleic acids in general (32). We aimed to investigate whether the shift in fluorescence intensity that was observed through flow cytometry was caused by a changing DNA or RNA content and in this way get more information about the cause of the observed phenotypic shift. Based on this tentative peak assignment, differences in nucleic acids between the coculture and the axenic populations were observed for both taxa (Fig. S6). However, there was no consistency in whether this was considered an increase or a decrease (i.e., for some wavenumbers the average intensity was higher in the coculture, while for other wavenumbers the intensity was higher in the axenic culture). When considering only uracil and thymine, it remained impossible to draw a conclusion regarding whether DNA or RNA differences contributed most to the observed phenotypic shift (Fig. S6).

DISCUSSION

There is an interest in understanding the implications of phenotypic heterogeneity in both natural and engineered microbial ecosystems. Our current knowledge is mainly based on experimental setups using axenic cultures. This is partly due to the fact that it is not straightforward to assess the phenotypic heterogeneity of an isogenic population in a mixed community. In order to circumvent this issue, we present a membrane-based synthetic community setup. Using this setup, we investigated the effect of microbial interactions on the individual phenotype and phenotypic diversities of the interacting taxa. To avoid modified behavior compared to behavior under natural conditions due to domestication history (33), two freshly isolated strains were used.

Effect of interaction on phenotype and phenotypic diversity. Based on flow cytometric fingerprinting, the phenotypic diversity of both community members was lower when they were grown in a coculture compared to when they were grown as axenic cultures (Fig. 2A; see Fig. S3 and S5 in the supplemental material). This effect of interaction on population diversity was more pronounced for *Enterobacter* than for *Pseudomonas*, indicating that different taxa had different phenotypic responses to the interaction. When comparing the populations through beta-diversity assessment (Fig. 3), a similar observation was found. The differences between the cytometric fingerprint of *Enterobacter* in the coculture and in the axenic culture were significant, whereas the differences between *Pseudomonas* in the coculture and in the axenic culture were not significant.

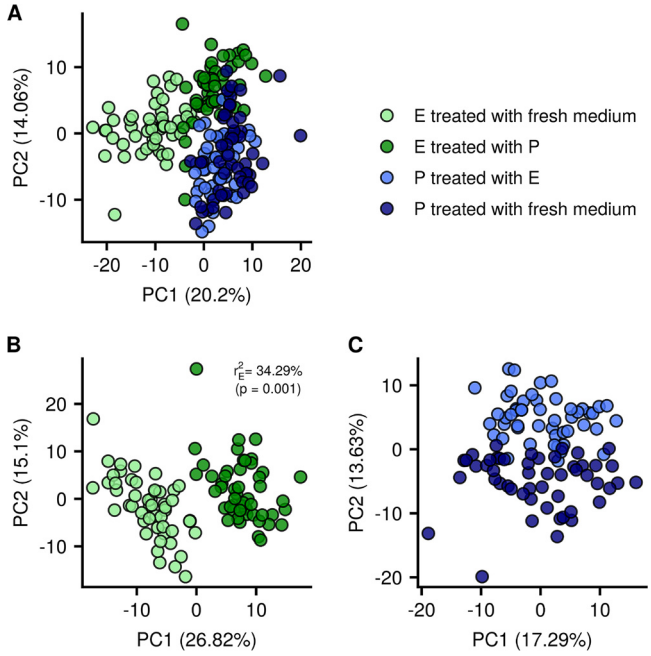

FIG 5 Visualization of the separability of the single-cell Raman spectra for *Enterobacter* and *Pseudomonas* in axenic culture and coculture at 72 h. There are 51 single-cell measurements for each population. The taxa are denoted as taxon E (*Enterobacter* sp.) and taxon P (*Pseudomonas* sp.), respectively. The populations are indicated with names in the form of "X treated with Y," where X is the taxon in the sample (E, P, or EP) and Y is what was present on the other side of the membrane (E, P, or fresh medium). PCA was carried out for the entire data set (A), for the spectra of *Enterobacter* separately (B), and for the spectra of *Pseudomonas* separately (C). The variance explained by the effect of coculturing compared to axenic culture (r^2_E) is provided for *Enterobacter* (PERMANOVA). Beta dispersions were differing significantly between the two groups, and therefore no PERMANOVA could be performed for *Pseudomonas*.

As indicated by the standard deviations that were found when calculating the average spectra for each population, Raman picks up a broad range of phenotypic diversity (Fig. S7 and S8). The data set with the single-cell Raman spectra was relatively small (i.e., 51 spectra per population). Diversity estimates are known to be sensitive to sample size (34). To be conservative, no conclusions were drawn regarding phenotypic diversity as observed using the single-cell Raman spectra. Similar to the flow cytometry results, PCA of the single-cell spectra indicated a bigger shift in phenotypes for *Enterobacter* and a smaller shift for *Pseudomonas*. The spectra of *Enterobacter* in the coculture and in the axenic culture were clearly separated (Fig. 5A). For *Pseudomonas*, the separation only became clear when the PCA was performed on the spectra for *Pseudomonas* alone (Fig. 5C). Since both techniques, flow cytometry and Raman spectroscopy, measure widely different optical properties of individual bacterial cells, finding the same observation using these two approaches strengthens confidence in the conclusions.

Differences in scattering patterns were limited for both taxa, implying that there were no large changes in cell morphology (35). Since SG staining is a stoichiometric staining, a higher fluorescence signal is directly related to a higher concentration of stained nucleic acids (36, 37). In terms of nucleic acid content, large differences were observed for *Enterobacter* and limited differences for *Pseudomonas*, with *Enterobacter* shifting toward high-nucleic-acid individuals (Fig. 2B and C; Fig. S5). This can indicate different physiological shifts. On the one hand, the DNA copy number could be increased, implying an adaptation of the cell cycle. Although both bacteria were expected to be in stationary phase at all sampling points (Fig. S9), it is possible that under stress the bacteria adapted their cell cycle behavior and DNA concentration (38). On the other hand, the bacteria might have maintained a similar DNA concentration but a higher RNA concentration, indicating a shift in their gene expression. The bacteria

could have been more actively expressing the same genes as they were in the axenic cultures, or they might have shifted toward expression of other genes compared to the axenic cultures (39). Lastly, an increased membrane permeability may also explain the higher fluorescence signals.

Through single-cell Raman spectroscopy, which offers an in-depth view on the biochemical phenotype, we attempted to investigate which of the above-mentioned scenarios was most likely to be occurring. Using a reference-based peak assignment, the Raman spectra indicated differences in wavenumbers that were potentially related to DNA and RNA and in this way support both hypotheses (Fig. S6). It should be noted that the tentative peak assignment resulted in inconsistent conclusions regarding the intensity change of nucleic-acid-related wavenumbers for both taxa under the different conditions (i.e., axenic or coculture). This might be explained by the fact that the signal intensity at every wavenumber is the superposition of all compounds' signals at this wavenumber, thereby prohibiting biomolecule-specific interpretation.

Several uptake or metabolic pathways are often simultaneously active in a single taxon's population (40, 41). Interspecies interactions are known to alter the intensity of the production pathways that are active in interacting bacteria (42, 43), and hence they may be influencing population heterogeneity. For example, the interspecies interactions may allow species to share products of costly pathways and in this way deprioritize some functions which would be necessary for the proliferation in monoculture, such as the production of certain amino acids (39, 42). Since costly production pathways are often expressed by only a fraction of a clonal population (15, 44), sharing these pathways between genotypes might allow one or both interacting genotypes to steer the distribution of their costly phenotypes and hence reduce their population heterogeneity. This would enable each genotype to occupy the functions at which it is most performant, thus creating a mixed community with a higher overall performance. The increased cell density in the mixed culture compared to the axenic cultures may indicate this increased performance (Fig. S2). The idea of pathway sharing is in line with the observation that the gene essentiality for a specific taxon is dependent on its community partners (45). It is possible that interactions between bacteria may indeed lead to other than only additive effects on the phenotypic population structure of the individual taxa. For example, a taxon that is excreting a certain metabolite may cause expression of metabolic pathways in taxa that utilize this metabolite and therefore affect the phenotypic diversity of these cross-feeding taxa. In addition to these cooperative interactions, competition may also explain the reduction in phenotypic diversity. It may confer a competitive advantage for a taxon to reduce its heterogeneity and in that way reduce the fraction of individuals that are in a suboptimal state for exploiting the current environmental conditions (13). In the present study, the community was predicted to be dominated by *Pseudomonas* (Fig. 4). A possible hypothesis for the fact that *Enterobacter* showed a stronger reduction in phenotypic diversity may be that *Enterobacter* needed to reduce its heterogeneity more in order to compete with *Pseudomonas*.

Evaluation of the experimental setup. In literature, phenotypic heterogeneity is most often studied though the assessment of single-cell metabolic activity, using isotope labeling with stable or radioactive probes (41, 46), or through the quantification of gene expression variability with fluorescence-labeled proteins (2, 11, 40). Both isotope labeling and fluorescence-labeled proteins allow the study of heterogeneity in clonal populations. However, these methods require either a modification of the organisms under study by inserting a fluorescent protein or the use of rather expensive, and sometimes dangerous, isotopes. Using phenotypic fingerprinting through flow cytometry does not require any tagging of bacteria or the use of isotopes. Moreover, it is possible to assess the phenotypic diversity of bacterial populations without prior knowledge on potentially relevant metabolic pathways (isotope labeling) or genes (fluorescence labeling). The main benefits of the flow cytometric approach are its speed and the fact that large amounts of cells can be analyzed. This allows good coverage of

the phenotypic landscape of the community and enables researchers to achieve a highly resolved sampling frequency.

However, when assessing phenotypic heterogeneity, there needs to be a definition of the phenotypes between which will be distinguished. Using the previously published protocol by Props et al. (47), a binning grid was applied to each of the bivariate parameter combinations (i.e., scatter and fluorescence parameters). Bacteria that fell within the same bin were defined as the same phenotype. Thus, phenotypes, and by extension the phenotypic diversity metrics, were defined *ad hoc*. Moreover, when evaluating phenotypic heterogeneity based on flow cytometry, the phenotypic traits on which information is gained are morphological parameters and nucleic acid content (in the case of SG staining). However, only a certain level of information is retained in the scatter and fluorescence parameters (e.g., morphology cannot be inferred directly from scatter values) (48). Thus, the phenotypic traits derived through flow cytometry are an abstract representation of the phenotype. In addition, only taking into account these traits is an abstraction of the entire phenotypic diversity of the bacteria. The fact that phenotypes were defined using a predefined binning grid and based on a limited number of phenotypic traits makes it difficult to make a link with functionality and to fully understand the underlying biological or ecological process that caused the phenotypic diversity shift. Additional examination of the transcriptome (39, 49, 50) or exometabolite profiles (51), or the use of mutant libraries, could provide valuable insights in the cause of the phenotypic adaptation and the functional consequences that the change in phenotypic state might bring. In addition, more validated and automated pipelines for detection of biomolecules based on single-cell Raman spectra would be an interesting improvement.

It should be noted that the difference in volume between the basal and apical phases may cause the metabolites consumed and produced to be slightly different compared to the mixed cultures. Differences in resource and metabolite concentration due to differences in total microbial load may have influenced the effect size of coculturing on the phenotypic diversity (52, 53). In addition, it should be noted that the current experimental setup assesses well-mixed communities. However, in nature, bacteria often occur in biofilms. In the case of mixed-species biofilms, the residing species would occur in "patches" where they would experience different microenvironmental conditions (e.g., due to diffusion-mediated distribution of nutrients, metabolites, etc.). Phenotypic heterogeneity in the center of a patch might then be mediated by intraspecies cell-to-cell interaction, while phenotypic heterogeneity on the edges of a patch may be mediated by interspecies cell-to-cell interactions. Further research to address these aspects is required.

Conclusion. In conclusion, we have used a synthetic community setup in which the individual phenotypic heterogeneity of environmental isolates in mixed or synthetic communities can be studied. We demonstrated that interactions between bacterial populations lead to an adjustment of the individual phenotypic diversities of the interacting populations. Since phenotypic heterogeneity is playing an important role in pathogenicity and virulence (14), antibiotic resistance (12, 54), biotechnological applications (20, 23, 55, 56), and ecosystem properties (57), it is crucial to understand its influencing factors. The experimental design presented here provides a framework within which further ecological hypotheses regarding phenotypic heterogeneity and microbial interactions can be tested.

MATERIALS AND METHODS

Isolates. An *Enterobacter* sp. and a *Pseudomonas* sp. were selected from a set of drinking water isolates which were isolated on R2A agar and provided by Pidpa (Provinciale en Intercommunale Drinkwatermaatschappij der Provincie Antwerpen, Antwerp, Belgium). Preliminary tests showed that these isolates had distinct cytometric fingerprints, as determined by the method of Rubbens et al. (30), and reached stationary growth phase within 24 h in M9 supplemented with 200 mg/liter glucose at 28°C, starting from a cell density of 10^6 cells ml^{-1} (Fig. S9). The isolates were identified with Sanger sequencing (LGC Genomics GmbH, Germany). DNA extraction was performed by means of bead beating with a PowerLyzer instrument (Qiagen, Venlo, Netherlands) and phenol-chloroform extraction. A PCR was performed on the V1 to V6 region of the 16S rRNA gene. The primers 63F (CAGGCCTAACACATGCAAGTC)

and 1378R (CGGTGTGTACAAGGCCCGGGAACG) were used, and amplification was performed using an initial denaturation for 5 min at 94°C, followed by 30 cycles of 1 min of denaturation at 95°C, 1 min of annealing at 53°C, and 2 min of extension at 72°C. A final elongation step was included at 72°C for 10 min. The quality of the PCR products was evaluated by agarose gel electrophoresis, and samples were sent out for Sanger sequencing. The obtained sequences were BLAST searched against two databases, NCBI BLAST and the Ribosomal Database Project (Table S2). Both databases yielded the same identities. The strains were deposited in the BCCM/LMG Bacteria Collection under accession numbers LMG 30741 (*Enterobacter* sp.) and LMG 30742 (*Pseudomonas* sp.).

Experimental setup. Bacteria were cultured in Transwell plates (Costar 6-well cell culture plates; Corning, Inc.), where apical and basal compartments were created using cell culture inserts (ThinCert cell culture inserts with pore diameters of 0.4 μm; Greiner Bio-One). The membranes of the culture inserts were replaced by membranes with smaller pore sizes to avoid migration of bacteria between the two compartments (Whatman Cyclopore polycarbonate and polyester membranes [0.2-μm pore size]; GE Life Sciences). Four synthetic communities were created: two axenic cultures, a physically separated culture, and a mixed culture (Fig. 1). Each community was prepared in triplicate and randomized over the plates to account for plate effects. Before the start of the experiment, both types of bacteria were grown on nutrient agar (Oxoid, UK) plates. For both taxa, a single colony was picked and transferred to liquid minimal medium (M9 with 200 mg/liter glucose as a carbon source). After 2 days of incubation at 28°C, the cell densities in the two liquid cultures were determined by flow cytometry, and the cultures were diluted to the desired starting cell densities in fresh medium in triplicate for each synthetic community. The required dilution was high enough to neglect differences in the volumes of fresh media and thus resources for growth that were needed to prepare the cultures. The starting cell densities were set to have the same initial cell density of 10^6 cells ml^{-1} in each synthetic community and with equal relative abundances for both community members in the cocultures and mixed cultures (Table S3). No additional medium was added after the initial setup of the experiment. The first sampling moment was at 24 h, which suggests, based on the previously determined growth kinetics, that both taxa were in stationary phase at every sampling point (Fig. S9). Interaction between the taxa was studied in stationary phase because previous research has indicated that both Raman spectroscopy and flow cytometry are able to pick up differences in phenotype and phenotypic community structure due to differences in growth stages. When bacterial populations are not standardized on growth phase, it would be difficult to distinguish between phenotypic diversity differences which are due to growth and differences which are due to the presence of the interacting partner taxon.

The six-well plates were incubated at 28°C and gently shaken (25 rpm) to aid diffusion of metabolites between the compartments. The communities were monitored over a period of 72 h. Every 24 h, the samples were analyzed by flow cytometry. After 72 h, the samples were fixed with 4% paraformaldehyde for Raman spectroscopic analysis (see the supplemental material). Sample fixation was necessary since single-cell Raman measurements were too time-consuming for immediate analysis.

Flow cytometry. For flow cytometric analysis, the samples were diluted and stained with 1 vol% SG (100× concentrate in 0.22-μm-filtered dimethyl sulfoxide; Invitrogen) for total cell analysis, and with 1 vol% SG combined with propidium iodide (SGPI; 100× concentrate SG [Invitrogen] and 50× 20 mM propidium iodide [Invitrogen] in 0.22-μm-filtered dimethyl sulfoxide) for Live/Dead analysis. SG primarily stains double-stranded DNA, but it will also stain the RNA (58). Staining was performed as described previously, with an incubation period of 20 min at 37°C in the dark (59). Samples were analyzed immediately after incubation on a FACSVerse flow cytometer (BD Biosciences, Belgium) equipped with eight fluorescence detectors (527/32, 783/56, 586/42, 700/54, 660/10, 783/56, 528/45, and 488/45 nm), two scatter detectors, and a blue 20-mW 488-nm laser, a red 40-mW 640-nm laser, and a violet 40-mW 405-nm laser. The flow cytometer was operated with FACSFlow solution (BD Biosciences) as sheath fluid. Instrument performance was verified daily using FACSuite CS&T beads (BD Biosciences).

Raman spectroscopy. Prior to analysis, the fixed sample was centrifuged for 5 min at room temperature and 5,000 × *g*, and the pellet was resuspended in 0.22-μm-filtered Milli-Q (4°C). A portion (10 μl) of cell suspension was spotted onto a CaF_2 slide (Crystran, Ltd., UK) and air dried for a few minutes. The dry sample was analyzed using an Alpha 300 R confocal Raman microscope (WITec GmbH, Germany) with a 100×/0.9NA objective (Nikon, Japan), a 785-nm excitation diode laser (Toptica, Germany), and a UHTS 300 spectrometer (WITec GmbH) with a −60°C cooled iDus 401 BR-DD charge-coupled device camera (Andor Technology, Ltd., UK). Laser power before the objective was measured daily and was about 150 mW. Spectra were acquired in the range of 110 to 3,375 cm^{-1} with a diffraction grating of 300 grooves/mm. For each single-cell spectrum, the Raman signal was integrated over 40 s. All Raman samples were analyzed within 1 week after sampling, with minimal time between them to limit possible differences caused by differences in storage duration. For each population, between 51 and 55 single-cell spectra were measured from a single biological replicate population. To allow for a fair comparison, 51 spectra were selected from each population for further analysis. The spectra with the lowest intensity were assumed to be of lesser quality and were therefore discarded.

A large peak in the range of 850 to 1,030 cm^{-1} was present in the spectra of *Enterobacter* in the axenic culture, while this peak was not observed in the other populations or during preliminary tests (Fig. S7). Moreover, intensity values showed large variability for this region. This might be the result of technical issues during fixation or storage of the sample. Similar to the study of García-Timermans et al. (60), this region was excluded for further analysis (Fig. S8).

Data analysis. (i) Flow cytometric diversity analysis. The flow cytometry data were imported in R (v3.3.1) (61) using the flowCore package (v1.40.3) (62). A quality control of the data set was performed through the flowAI package (v1.6.2) (63). The data were transformed using the arcsine hyperbolic

function, and the background of the fingerprints was removed by manually creating a gate on the primary fluorescent channels (59). The Phenoflow package (v1.1.1.) (47) was used to assess the phenotypic community structure of the bacterial populations. Based on the study by Rubbens et al. (64), which assessed the usefulness of information captured by additional detectors (i.e., detectors that are not directly targeted) for bacterial population identification, an optimal subset of detectors was selected to include in the analysis. The subset included the scatter detectors, the detector for which had been stained (i.e., fluorescein isothiocyanate), and some additional detectors that received spillover signals (AmCyan, dsRed, and eCFP).

Prior to diversity estimation, all populations were subsampled to 30,000 cells in order to account for sample size differences. In short, for each bivariate parameter combination (i.e., combination of the scatter and fluorescence parameters) an 128×128 equal-space binning grid is applied, which discretizes the parameter space and in which each bin represents a hypothetical phenotype. For each bin, a kernel density estimation is performed. All density estimations are summed to the total density estimation of the community. Finally, the density values for each of the bins are concatenated into a one-dimensional vector, which is called the "phenotypic fingerprint." From this fingerprint, alpha and beta diversities are calculated, which are then used as measures for phenotypic population heterogeneity. The alpha diversity (i.e., within-sample diversity) is calculated by using the first three Hill diversity numbers, D_0, D_1, and D_2, which correspond to the observed richness, the exponential of Shannon entropy, and the inverse Simpson index, respectively (65). The beta diversity (i.e., between-sample diversity) is evaluated by PCoA on the Bray-Curtis dissimilarities between the fingerprints. The significance of the differences between fingerprints was assessed by means of PERMANOVA (999 permutations) on the Bray-Curtis dissimilarity matrix. The homogeneity of variance in groups was assessed before performing PERMANOVA. A significance level of 0.01 was used.

(ii) Flow cytometric *in silico* communities. Relative abundances in the mixed cultures were predicted using the supervised *in silico* community methodology of Rubbens et al. (64), implemented in the Phenoflow (v1.1.1) software package. In short, a cytometric fingerprint of the taxa that make up the synthetic community is made. Next, the single-cell data of the axenic cultures are aggregated to a so-called "*in silico* community." This *in silico* community consists of labeled data, which allows the use of supervised machine learning techniques, such as random forests, to discriminate between different community members. The label to be predicted is the taxon, and the predictors are the scatter and fluorescence parameters. Once this classifier has been trained on the data set, it can use the single-cell data to predict the relative abundances of both taxa in a mixture. For training of the random forests, the biological replicates were pooled, and 10,000 cells of both *Enterobacter* and *Pseudomonas* were randomly sampled.

(iii) Raman spectra. The Raman spectrum data were analyzed in R (v3.3.1). Spectral processing was adapted from the study of Berry et al. (66) and was performed using the MALDIquant package (v1.16) (67). In short, a baseline correction was performed using the statistics-sensitive nonlinear iterative peak-clipping (SNIP) algorithm. Next, the biologically relevant part of the spectrum (600 to 1,800 cm^{-1}) was selected (25), and the spectra were normalized by surface normalization. The intensity values were zero centered and scaled to unit variance before performing PCA (statistical package, v3.3.4).

Data availability. The entire data analysis pipeline is available as an R Markdown document at https://github.com/jeheyse/Cocultures2018. The Raman data and accompanying metadata are available at https://github.com/jeheyse/Cocultures2018. Raw FCM data and metadata are available on FlowRepository under accession ID FR-FCM-ZYWN.

SUPPLEMENTAL MATERIAL

Supplemental material for this article may be found at https://doi.org/10.1128/AEM.02814-18.

SUPPLEMENTAL FILE 1, PDF file, 5.3 MB.

ACKNOWLEDGMENTS

We thank Katrien De Maeyer (Pidpa) for providing the isolates. We thank Tom Bellon for assistance during the flow cytometric measurements and Dmitry Khalenkow for assistance in the Raman spectroscopy measurements.

This study was supported through the Geconcentreerde Onderzoeksactie (GOA) from Ghent University (BOF15/GOA/006). J.H. is supported by the Flemish Fund for Scientific Research (FWO-Vlaanderen, project 1S80618N). B.B. is supported by the Institute for Innovation by Science and Technology in Flanders (IWT, project 131370). R.P. is supported by Ghent University (BOFDOC2015000601). P.R. is supported by Ghent University (BOFSTA2015000501). A.G.S. acknowledges the support of Ghent University (BOF14/IOP/003, BAS094-18, and 01IO3618) and the Flemish Fund for Scientific Research (FWO-Vlaanderen, G043219).

J.H., R.P., P.R., B.B., A.G.S., W.W., and N.B. conceived the study. J.H. carried out the laboratory work and analyzed the data. J.H., B.B., R.P., and P.R. interpreted the results and wrote the paper. N.B., W.W., and A.G.S. supervised the findings of this work. All authors reviewed and approved the manuscript.

The authors declare that there are no conflicts of interest.

REFERENCES

1. Spudich JL, Koshland DE. 1976. Non-genetic individuality: chance in the single cell. Nature 262:467–471. https://doi.org/10.1038/262467a0.
2. Elowitz MB, Levine AJ, Siggia ED, Swain PS. 2002. Stochastic gene expression in a single cell. Science 297:1183–1186. https://doi.org/10.1126/science.1070919.
3. Rainey PB, Kerr B. 2010. Cheats as first propagules: a new hypothesis for the evolution of individuality during the transition from single cells to multicellularity. Bioessays 32:872–880. https://doi.org/10.1002/bies.201000039.
4. Govers SK, Adam A, Blockeel H, Aertsen A. 2017. Rapid phenotypic individualization of bacterial sister cells. Sci Rep 7:1–9. https://doi.org/10.1038/s41598-017-08660-0.
5. Ackermann M. 2015. A functional perspective on phenotypic heterogeneity in microorganisms. Nat Rev Microbiol 13:497–508. https://doi.org/10.1038/nrmicro3491.
6. Raser JM, O'Shea EK. 2005. Noise in gene expression: origins, consequences, and control. Science 309:2010–2013. https://doi.org/10.1126/science.1105891.
7. Avery SV. 2006. Microbial cell individuality and the underlying sources of heterogeneity. Nat Rev Microbiol 4:577–587. https://doi.org/10.1038/nrmicro1460.
8. Ansel J, Bottin H, Rodriguez-Beltran C, Damon C, Nagarajan M, Fehrmann S, François J, Yvert G. 2008. Cell-to-cell stochastic variation in gene expression is a complex genetic trait. PLoS Genet 4:1–10. https://doi.org/10.1371/journal.pgen.1000049.
9. Fraser D, Kaern M. 2009. A chance at survival: gene expression noise and phenotypic diversification strategies. Mol Microbiol 71:1333–1340. https://doi.org/10.1111/j.1365-2958.2009.06605.x.
10. Ozbudak EM, Thattai M, Kurtser I, Grossman AD, van Oudenaarden A. 2002. Regulation of noise in the expression of a single gene. Nat Genet 31:69–73. https://doi.org/10.1038/ng869.
11. Newman JRS, Ghaemmaghami S, Ihmels J, Breslow DK, Noble M, DeRisi JL, Weissman JS. 2006. Single-cell proteomic analysis of *Saccharomyces cerevisiae* reveals the architecture of biological noise. Nature 441:840–846. https://doi.org/10.1038/nature04785.
12. Balaban NQ, Merrin J, Chait R, Kowalik L, Leibler S. 2004. Bacterial persistence as a phenotypic switch. Science 305:1622–1626. https://doi.org/10.1126/science.1099390.
13. Acar M, Mettetal JT, Van Oudenaarden A. 2008. Stochastic switching as a survival strategy in fluctuating environments. Nat Genet 40:471–475. https://doi.org/10.1038/ng.110.
14. Ackermann M, Stecher B, Freed NE, Songhet P, Hardt W-D, Doebeli M. 2008. Self-destructive cooperation mediated by phenotypic noise. Nature 454:987–990. https://doi.org/10.1038/nature07067.
15. Veening JW, Igoshin OA, Eijlander RT, Nijland R, Hamoen LW, Kuipers OP. 2008. Transient heterogeneity in extracellular protease production by *Bacillus subtilis*. Mol Syst Biol 4:1–15. https://doi.org/10.1038/msb.2008.18.
16. Rosenthal AZ, Qi Y, Hormoz S, Park J. 2018. Metabolic interactions between dynamic bacterial subpopulations. Elife 7:1–18. https://doi.org/10.7554/eLife.33099.
17. Ackermann M. 2013. Microbial individuality in the natural environment. ISME J 7:465–467. https://doi.org/10.1038/ismej.2012.131.
18. Ackermann M, Schreiber F. 2015. A growing focus on bacterial individuality. Environ Microbiol 17:2193–2195. https://doi.org/10.1111/1462-2920.12877.
19. Zimmermann M, Escrig S, Hübschmann T, Kirf MK, Brand A, Inglis RF, Musat N, Müller S, Meibom A, Ackermann M, Schreiber F. 2015. Phenotypic heterogeneity in metabolic traits among single cells of a rare bacterial species in its natural environment quantified with a combination of flow cell sorting and NanoSIMS. Front Microbiol 6:1–11. https://doi.org/10.3389/fmicb.2015.00243.
20. Sheik AR, Muller EEL, Audinot JN, Lebrun LA, Grysan P, Guignard C, Wilmes P. 2016. *In situ* phenotypic heterogeneity among single cells of the filamentous bacterium *Candidatus* Microthrix parvicella. ISME J 10:1274–1279. https://doi.org/10.1038/ismej.2015.181.
21. Brehm-Stecher BF, Johnson EA. 2004. Single-cell microbiology: tools, technologies, and applications. Microbiol Mol Biol Rev 68:538–559. https://doi.org/10.1128/MMBR.68.3.538-559.2004.
22. Davis KM, Isberg RR. 2016. Defining heterogeneity within bacterial populations via single cell approaches. Bioessays 38:782–790. https://doi.org/10.1002/bies.201500121.
23. González-Cabaleiro R, Mitchell AM, Smith W, Wipat A, Ofiteru ID. 2017. Heterogeneity in pure microbial systems: experimental measurements and modeling. Front Microbiol 8:1–8. https://doi.org/10.3389/fmicb.2017.01813.
24. Nebe-Von-Caron G, Stephens PJ, Hewitt CJ, Powell JR, Badley RA. 2000. Analysis of bacterial function by multi-colour fluorescence flow cytometry and single cell sorting. J Microbiol Methods 42:97–114. https://doi.org/10.1016/S0167-7012(00)00181-0.
25. Read DS, Woodcock DJ, Strachan NJC, Forbes KJ, Colles FM, Maiden MCJ, Clifton-Hadley F, Ridley A, Vidal A, Rodgers J, Whiteley AS, Sheppard K. 2013. Evidence for phenotypic plasticity among multihost *Campylobacter jejuni* and *C. coli* lineages, obtained using ribosomal multilocus sequence typing and Raman spectroscopy. Appl Environ Microbiol 79:965–973. https://doi.org/10.1128/AEM.02521-12.
26. van de Vossenberg J, Tervahauta H, Maquelin K, Blokker-Koopmans CHW, Uytewaal-Aarts M, van der Kooij D, van Wezel AP, van der Gaag B. 2013. Identification of bacteria in drinking water with Raman. Anal Methods 5:2679–2687. https://doi.org/10.1039/c3ay40289d.
27. De Roy K, Marzorati M, Van den Abbeele P, Van de Wiele T, Boon N. 2014. Synthetic microbial ecosystems: an exciting tool to understand and apply microbial communities. Environ Microbiol 16:1472–1481. https://doi.org/10.1111/1462-2920.12343.
28. Jessup CM, Kassen R, Forde SE, Kerr B, Buckling A, Rainey PB, Bohannan BJM. 2004. Big questions, small worlds: microbial model systems in ecology. Trends Ecol Evol 19:189–197. https://doi.org/10.1016/j.tree.2004.01.008.
29. Goers L, Freemont P, Polizzi KM. 2014. Coculture systems and technologies: taking synthetic biology to the next level. J R Soc Interface 11:1–13. https://doi.org/10.1098/rsif.2014.0065.
30. Rubbens P, Props R, Boon N, Waegeman W. 2017. Flow cytometric single-cell identification of populations in synthetic bacterial communities. PLoS One 12:1–19. https://doi.org/10.1371/journal.pone.0169754.
31. De Gelder J, Gussem KD, Vandenabeele P, Moens L. 2007. Reference database of Raman spectra of biological molecules. J Raman Spectrosc 38:1133–1147. https://doi.org/10.1002/jrs.1734.
32. Teng L, Wang X, Wang X, Gou H, Ren L, Wang T, Wang Y, Ji Y, Huang WE, Xu J. 2016. Label-free, rapid and quantitative phenotyping of stress response in *Escherichia coli* via ramanome. Sci Rep 6:34359–34310. https://doi.org/10.1038/srep34359.
33. Yu Z, Krause SMB, Beck DAC, Chistoserdova L. 2016. A synthetic ecology perspective: how well does behavior of model organisms in the laboratory predict microbial activities in natural habitats? Front Microbiol 7:1–7. https://doi.org/10.3389/fmicb.2016.00946.
34. Gotelli NJ, Colwell RK. 2001. Quantifying biodiversity procedures and pitfalls in the measurement and comparison of species richness. Ecol Lett 4:379–391. https://doi.org/10.1046/j.1461-0248.2001.00230.x.
35. Gatza E, Hammes F, Prest E. 2013. Assessing water quality with the BD Accuri™ C6 flow cytometer. BD Biosciences white paper. BD Biosciences, San Jose, CA.
36. Berney M, Hammes F, Bosshard F, Weilenmann HU, Egli T. 2007. Assessment and interpretation of bacterial viability by using the Live/Dead BacLight kit in combination with flow cytometry. Appl Environ Microbiol 73:3283–3290. https://doi.org/10.1128/AEM.02750-06.
37. Müller S, Nebe-Von-Caron G. 2010. Functional single-cell analyses: flow cytometry and cell sorting of microbial populations and communities. FEMS Microbiol Rev 34:554–587. https://doi.org/10.1111/j.1574-6976.2010.00214.x.
38. Lieder S, Jahn M, Koepff J, Müller S, Takors R. 2016. Environmental stress speeds up DNA replication in *Pseudomonas putida* in chemostat cultivations. Biotechnol J 11:155–163. https://doi.org/10.1002/biot.201500059.
39. Hansen LBS, Ren D, Burmølle M, Sørensen SJ. 2017. Distinct gene expression profile of *Xanthomonas retroflexus* engaged in synergistic multispecies biofilm formation. ISME J 11:300–303. https://doi.org/10.1038/ismej.2016.107.
40. Nikolic N, Barner T, Ackermann M. 2013. Analysis of fluorescent reporters indicates heterogeneity in glucose uptake and utilization in clonal bacterial populations. BMC Microbiol 13:258–270. https://doi.org/10.1186/1471-2180-13-258.
41. Schreiber F, Littmann S, Lavik G, Escrig S, Meibom A, Kuypers MMM,

Ackermann M. 2016. Phenotypic heterogeneity driven by nutrient limitation promotes growth in fluctuating environments. Nat Microbiol 1:1–7. https://doi.org/10.1038/nmicrobiol.2016.55.
42. Pande S, Merker H, Bohl K, Reichelt M, Schuster S, De Figueiredo LF, Kaleta C, Kost C. 2014. Fitness and stability of obligate cross-feeding interactions that emerge upon gene loss in bacteria. ISME J 8:953–962. https://doi.org/10.1038/ismej.2013.211.
43. Vaz Jauri P, Kinkel LL. 2014. Nutrient overlap, genetic relatedness and spatial origin influence interaction-mediated shifts in inhibitory phenotype among *Streptomyces* spp. FEMS Microbiol Ecol 90:264–275. https://doi.org/10.1111/1574-6941.12389.
44. van Gestel J, Nowak MA. 2016. Phenotypic heterogeneity and the evolution of bacterial life cycles. PLoS Comput Biol 12:1–23. https://doi.org/10.1371/journal.pcbi.1004764.
45. Ibberson CB, Stacy A, Fleming D, Dees JL, Rumbaugh K, Gilmore MS, Whiteley M. 2017. Coinfecting microorganisms dramatically alter pathogen gene essentiality during polymicrobial infection. Nat Microbiol 2:1–6. https://doi.org/10.1038/nmicrobiol.2017.79.
46. Wang Y, Huang WE, Cui L, Wagner M. 2016. Single cell stable isotope probing in microbiology using Raman microspectroscopy. Curr Opin Biotechnol 41:34–42. https://doi.org/10.1016/j.copbio.2016.04.018.
47. Props R, Monsieurs P, Mysara M, Clement L, Boon N. 2016. Measuring the biodiversity of microbial communities by flow cytometry. Methods Ecol Evol 7:1376–1385. https://doi.org/10.1111/2041-210X.12607.
48. Fontana S, Jokela J, Pomati F. 2014. Opportunities and challenges in deriving phytoplankton diversity measures from individual trait-based data obtained by scanning flow cytometry. Front Microbiol 5:1–12. https://doi.org/10.3389/fmicb.2014.00324.
49. González-Torres P, Pryszcz LP, Santos F, Martínez-García M, Gabaldón T, Antón J. 2015. Interactions between closely related bacterial strains are revealed by deep transcriptome sequencing. Appl Environ Microbiol 81:8445–8456. https://doi.org/10.1128/AEM.02690-15.
50. Schulze S, Schleicher J, Guthke R, Linde J. 2016. How to predict molecular interactions between species? Front Microbiol 7:1–13. https://doi.org/10.3389/fmicb.2016.00442.
51. Chodkowski JL, Shade A. 2017. A new synthetic community system for probing microbial interactions driven by exometabolites. mSystems 2:1–14. https://doi.org/10.1128/mSystems.00129-17.
52. Anetzberger C, Pirch T, Jung K. 2009. Heterogeneity in quorum sensing-regulated bioluminescence of *Vibrio harveyi*. Mol Microbiol 73:267–277. https://doi.org/10.1111/j.1365-2958.2009.06768.x.
53. Pérez PD, Hagen SJ. 2010. Heterogeneous response to a quorum-sensing signal in the luminescence of individual *Vibrio fischeri*. PLoS One 5:1–9. https://doi.org/10.1371/journal.pone.0015473.
54. Wiuff C, Zappala RM, Regoes RR, Garner KN, Baquero F, Levin BR. 2005. Phenotypic tolerance: antibiotic enrichment of noninherited resistance in bacterial populations. Antimicrob Agents Chemother 49:1483–1494. https://doi.org/10.1128/AAC.49.4.1483-1494.2005.
55. Lencastre Fernandes R, Nierychlo M, Lundin L, Pedersen AE, Puentes Tellez PE, Dutta A, Carlquist M, Bolic A, Schäpper D, Brunetti AC, Helmark S, Heins AL, Jensen AD, Nopens I, Rottwitt K, Szita N, van Elsas JD, Nielsen PH, Martinussen J, Sørensen SJ, Lantz AE, Gernaey KV. 2011. Experimental methods and modeling techniques for description of cell population heterogeneity. Biotechnol Adv 29:575–599. https://doi.org/10.1016/j.biotechadv.2011.03.007.
56. Delvigne F, Goffin P. 2014. Microbial heterogeneity affects bioprocess robustness: dynamic single-cell analysis contributes to understanding of microbial populations. Biotechnol J 9:61–72. https://doi.org/10.1002/biot.201300119.
57. Fontana S, Thomas MK, Moldoveanu M, Spaak P, Pomati F. 2018. Individual-level trait diversity predicts phytoplankton community properties better than species richness or evenness. ISME J 12:356–366. https://doi.org/10.1038/ismej.2017.160.
58. Johnson I, Spence MTZ. 2010. The molecular probes handbook: a guide to fluorescent probes and labeling technologies. Life Technologies Corporation, Carlsbad, CA.
59. Prest EI, Hammes F, Kötzsch S, van Loosdrecht MCM, Vrouwenvelder JS. 2013. Monitoring microbiological changes in drinking water systems using a fast and reproducible flow cytometric method. Water Res 47:7131–7142. https://doi.org/10.1016/j.watres.2013.07.051.
60. García-Timermans C, Rubbens P, Kerckhof FM, Buysschaert B, Khalenkow D, Waegeman W, Skirtach AG, Boon N. 2018. Label-free Raman characterization of bacteria calls for standardized procedures. J Microbiol Methods 151:69–75. https://doi.org/10.1016/j.mimet.2018.05.027.
61. R Core Team. 2017. R: a language and environment for statistical computing. R Foundation for Statistical Computing, Vienna, Austria.
62. Hahne F, LeMeur N, Brinkman RR, Ellis B, Haaland P, Sarkar D, Spidlen J, Strain E, Gentleman R. 2009. flowCore: a bioconductor package for high throughput flow cytometry. BMC Bioinformatics 10:106–108. https://doi.org/10.1186/1471-2105-10-106.
63. Monaco G, Chen H, Poidinger M, Chen J, De Magalhães JP, Larbi A. 2016. flowAI: automatic and interactive anomaly discerning tools for flow cytometry data. Bioinformatics 32:2473–2480. https://doi.org/10.1093/bioinformatics/btw191.
64. Rubbens P, Props R, Garcia-Timermans C, Boon N, Waegeman W. 2017. Stripping flow cytometry: how many detectors do we need for bacterial identification? Cytometry 91:1184–1191. https://doi.org/10.1002/cyto.a.23284.
65. Hill MO. 1973. Diversity and evenness: a unifying notation and its consequences. Ecology 54:427–432. https://doi.org/10.2307/1934352.
66. Berry D, Mader E, Lee TK, Woebken D, Wang Y, Zhu D, Palatinszky M, Schintlmeister A, Schmid MC, Hanson BT, Shterzer N, Mizrahi I, Rauch I, Decker T, Bocklitz T, Popp J, Gibson CM, Fowler PW, Huang WE, Wagner M. 2015. Tracking heavy water (D_2O) incorporation for identifying and sorting active microbial cells. Proc Natl Acad Sci U S A 112:194–203. https://doi.org/10.1073/pnas.1420406112.
67. Gibb S, Strimmer K. 2012. MALDIquant: a versatile R package for the analysis of mass spectrometry data. Bioinformatics 28:2270–2271. https://doi.org/10.1093/bioinformatics/bts447.